Deformable Thermo-Responsive Smart Windows Based on a Shape Memory Polymer for Adaptive Solar Modulations

Dan Li, [1‡] Chengzhi Zhou, [1,2‡] Yun Meng, [1] Chao Chen, [1] Chengjiao Yu, [3] Yi Long, [1]* Shuzhou Li[1]*

1. School of Materials Science and Engineering, Nanyang Technological University, 50 Nanyang Avenue, Singapore 639798, Singapore

2. Energy Research Institute @ NTU, Interdisciplinary Graduate School, Nanyang Technological University, 50 Nanyang Drive, 637553, Singapore.

3. School of Mechanical Engineering, Hebei University of Technology, Tianjin City, China, 300401

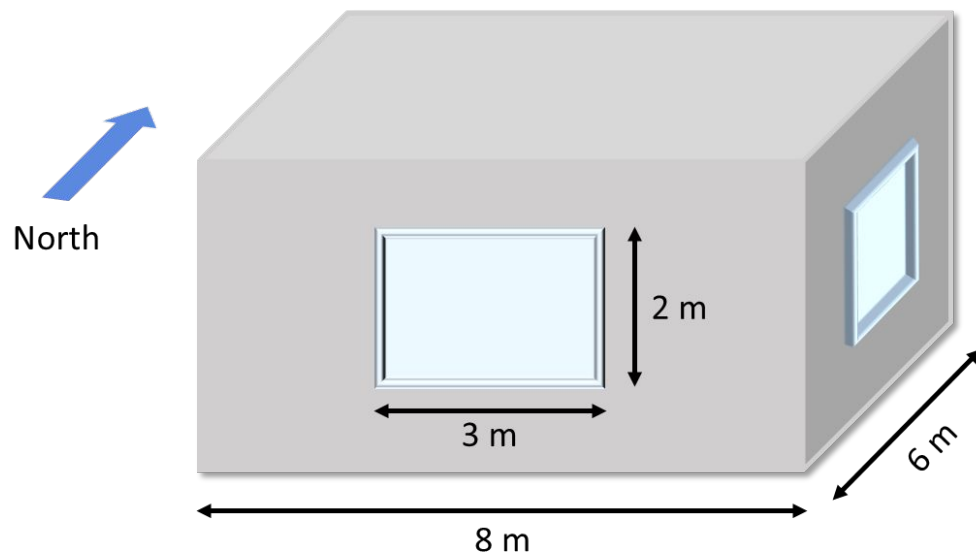Corresponding Author

*Email: longyi@ntu.edu.sg; lisz@ntu.edu.sg

Figure S1. Schematic demonstration of the house model used for energy-saving performance simulation.
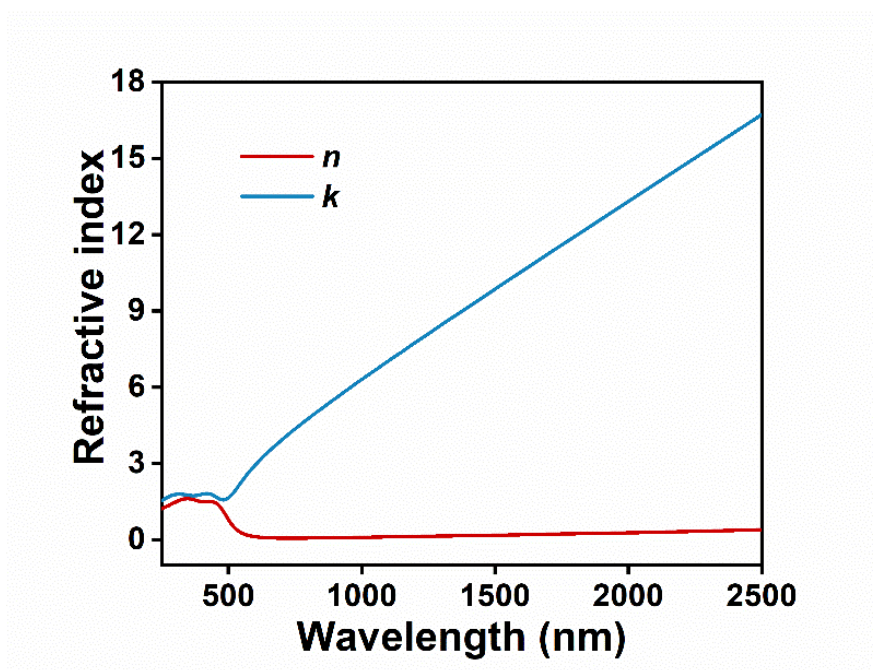
Figure S2. The optical constants (refractive index *n* and extinction coefficient *k*) of Au.
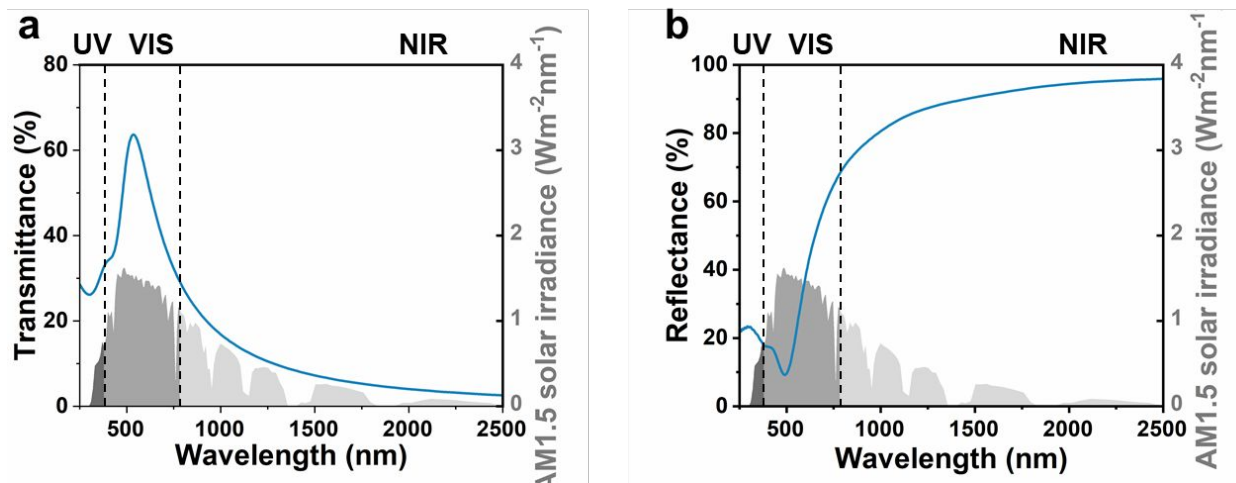
Figure S3. Simulated UV-vis-NIR transmittance (a) and reflectance (b) spectra of Au film with 20 nm thickness.
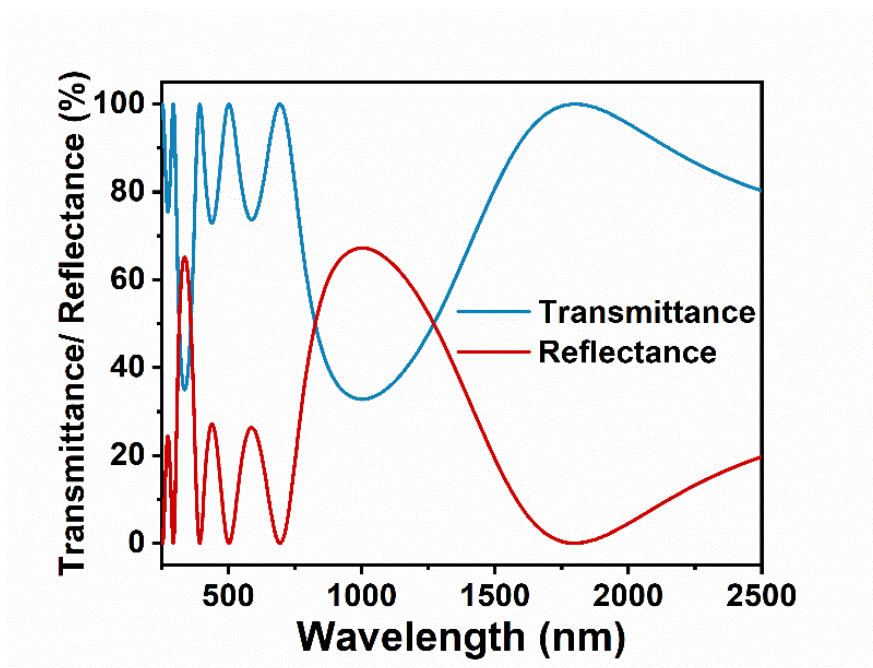
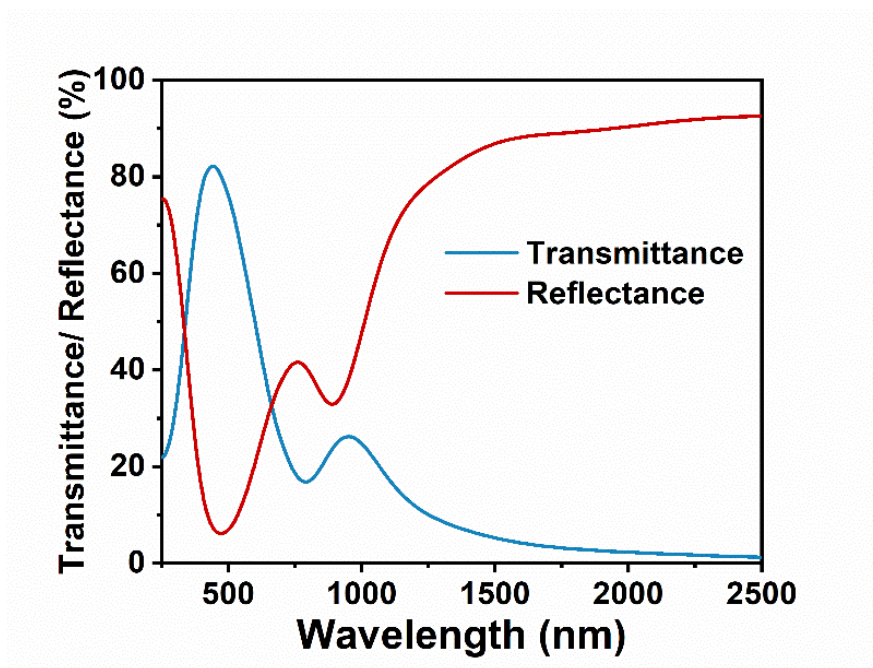**Figure S4.** Simulated UV-vis-NIR transmittance and reflectance spectra of TiO_2/SiO_2/TiO_2 films.

Figure S5. Simulated UV-vis-NIR transmittance and reflectance spectra of TiO_2/Al/TiO_2 film.
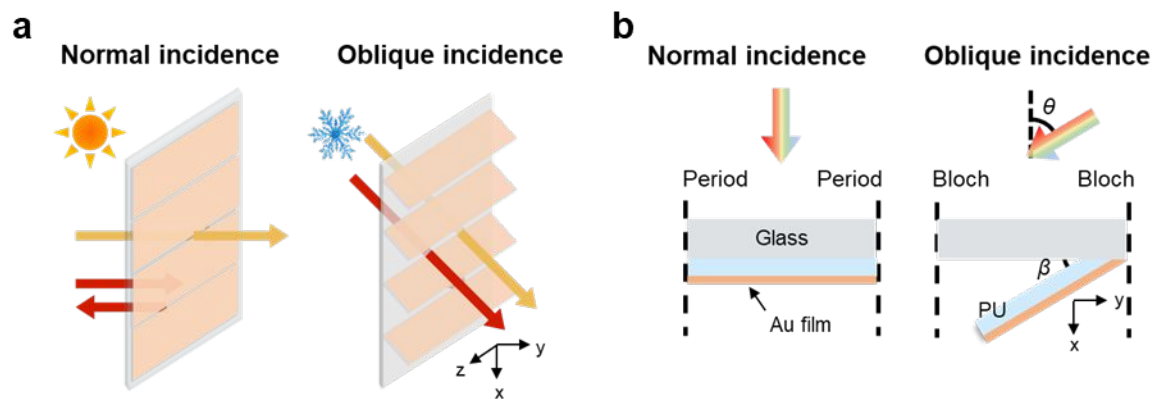
Figure S6. a) The schematic illustration of the three-dimensional geometry structures of the BSW in summer and winter. (b) The FDTD simulation model of the BSW with two-dimensional geometry structures in summer and winter. One repeating unit is simulated since the BSW is periodic along the x-axis.
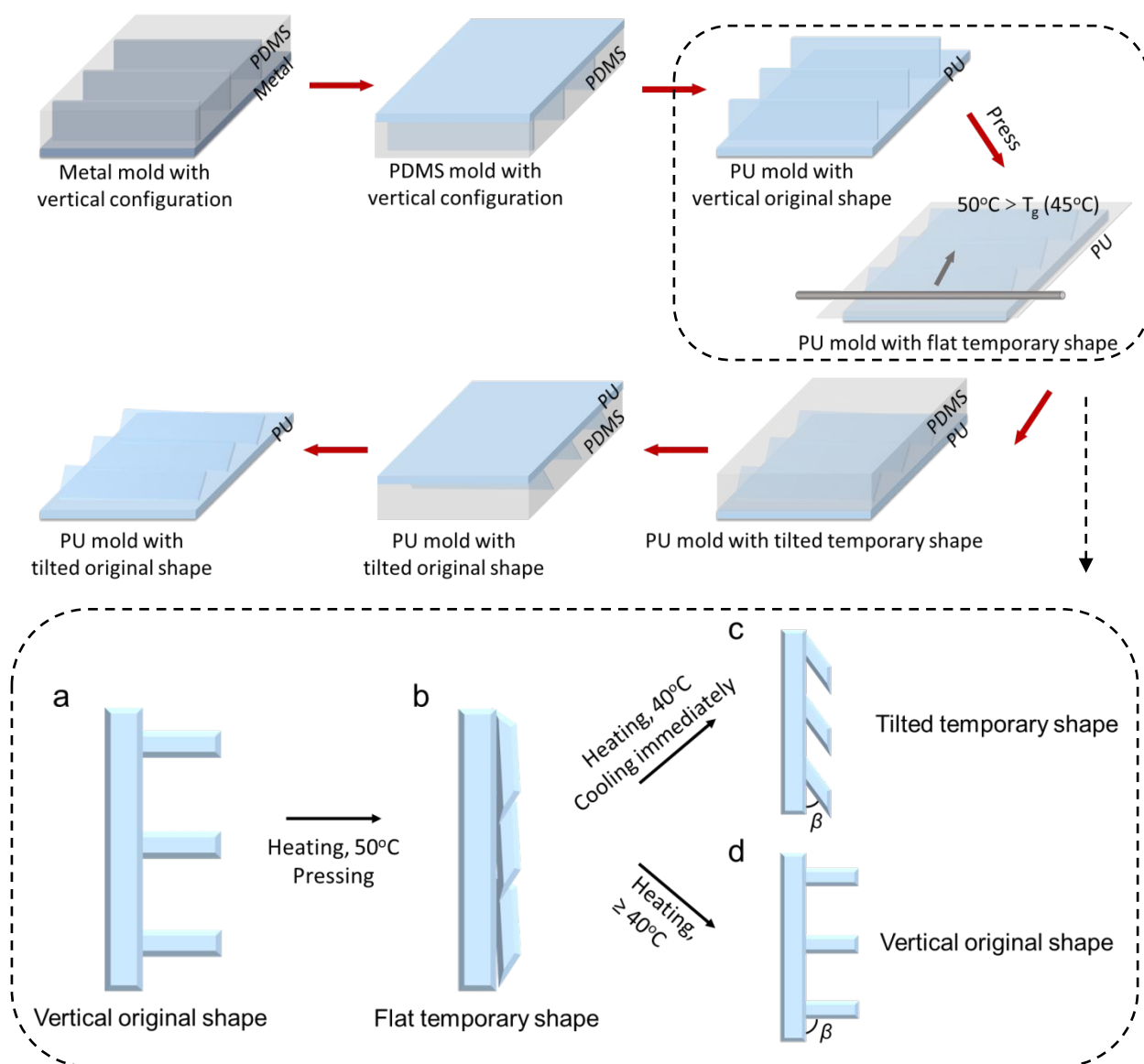
Figure S7. The schematic diagram of the preparation processes of the PU mold with tilted original shape. The schematic diagram in the dashed box shows the preparation processes of the PU mold with tilted temporary shape. (a) The PU mold with vertical original shape. (b) The PU mold with flat temporary shape (c) The PU mold with tilted temporary shape. (d) The PU mold with vertical original shape.
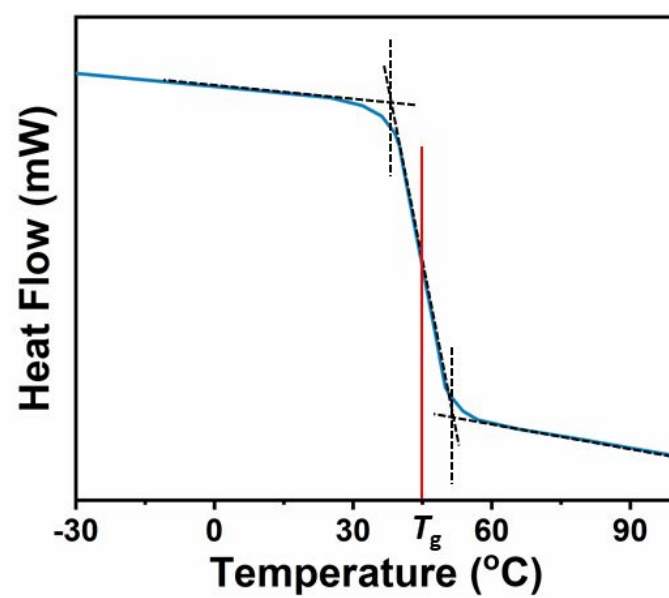
Figure S8. The T_g temperature of PU analysed by the differential scanning calorimetry.
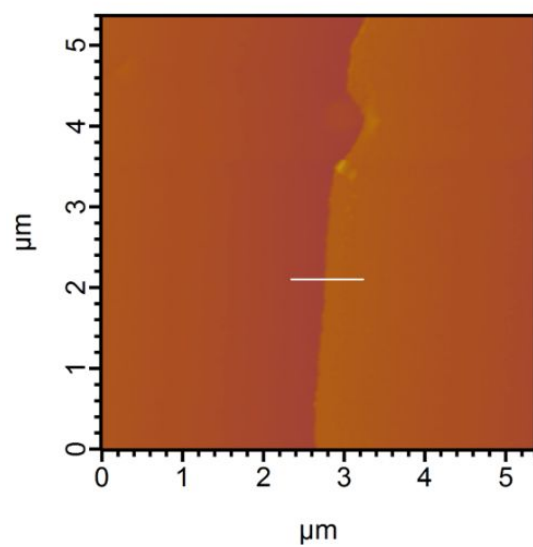
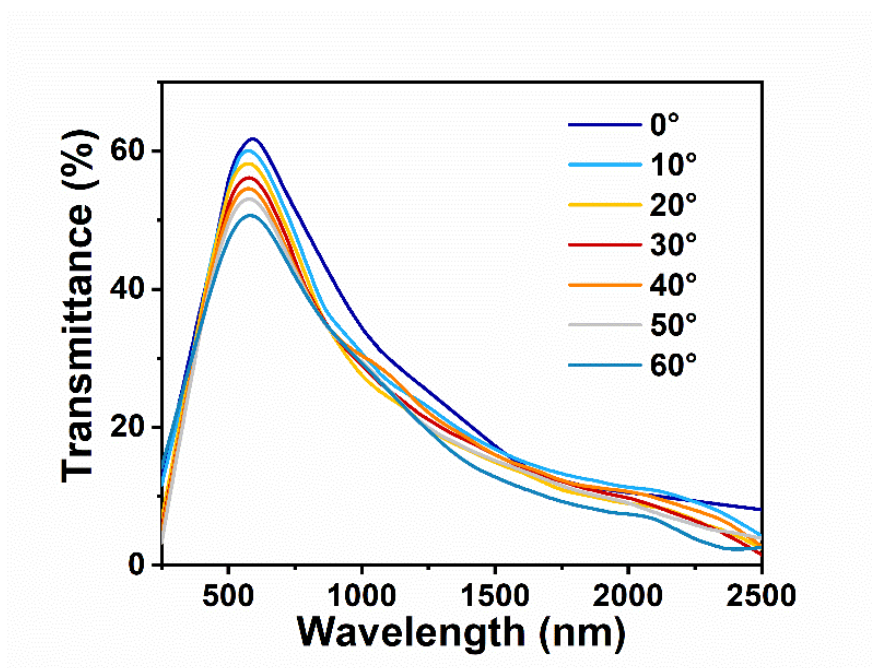**Figure S9.** The AFM image of Au films with 20 nm thickness.

Figure S10. UV-vis-NIR transmittance spectra of Au film with different incident angles.
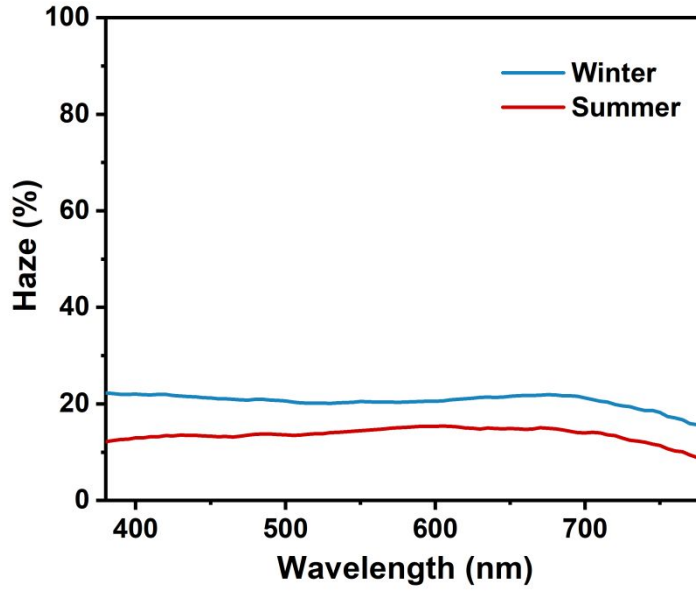
Figure S11. The optical haze of the BSW in winter and summer, respectively.

The optical haze of the BSW was measured through the Lambda 950 UV–vis–NIR spectrophotometer system fitted with the integration sphere according to ASTM D1003 "Standard Test Method for Haze and Luminous Transmittance of Transparent Plastics",[1] and is calculated as

$$\text{Haze\%} = \left(\frac{T_4}{T_2} - \frac{T_3}{T_1}\right) \times 100 \qquad (1)$$

There, T_2 refers to the total light transmitted by the specimen, and T_1 refers to the incident light. T_4 refers to the light scattered by the instrument and specimen and T_3 refers to the light scattered by the instrument.
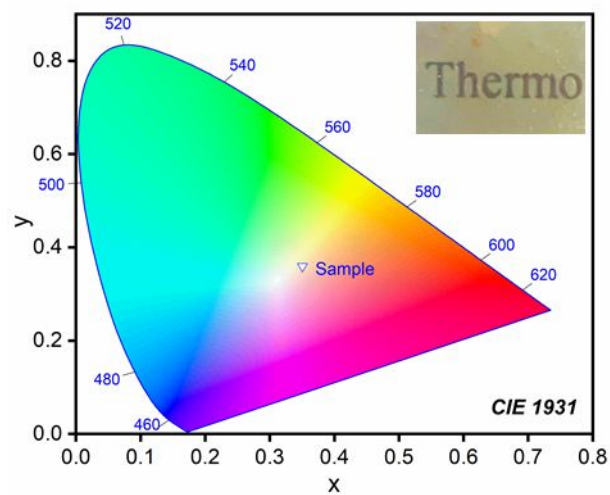
Figure S12. The color distribution of the Au coated PU film in the CIE chromaticity diagram. The insert is the picture of the Au coated PU film.
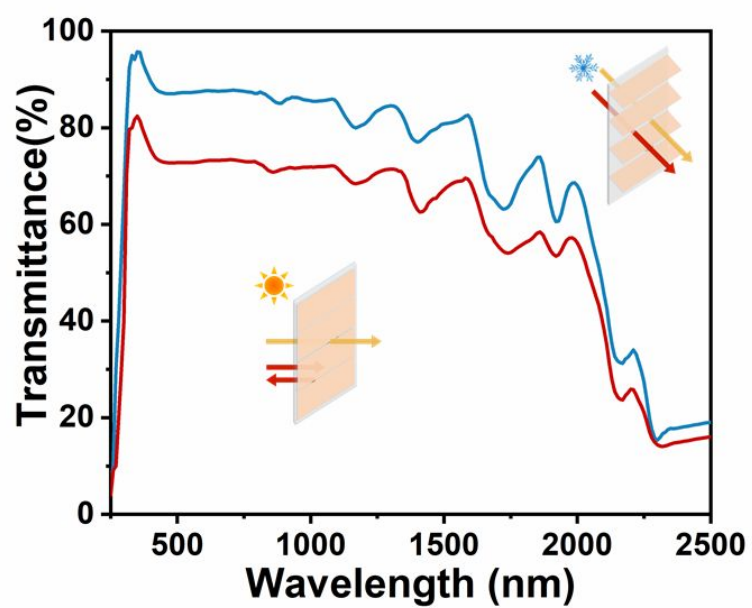
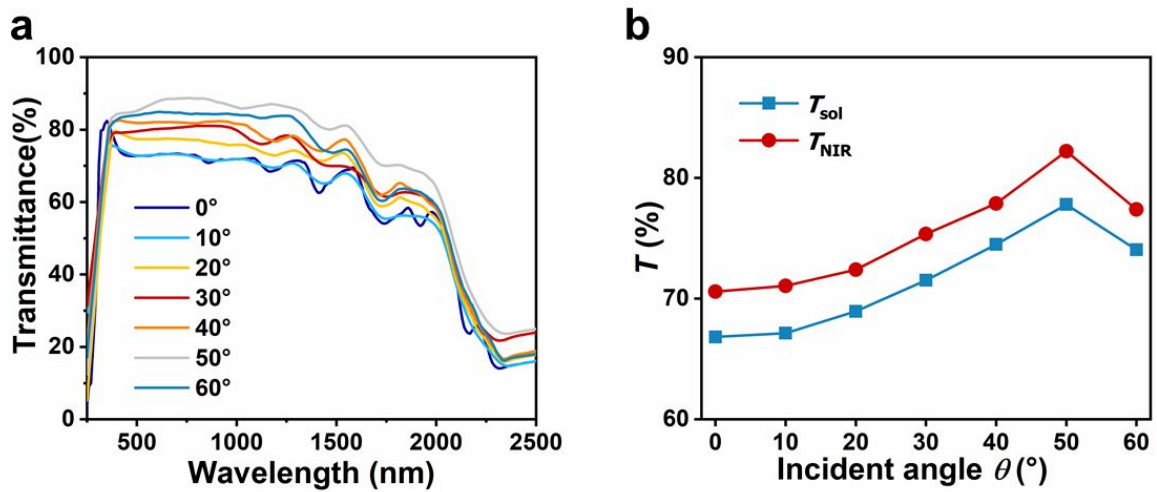**Figure S13.** The UV-vis-NIR transmittance spectra of the BSW without Au film in summer and winter.

Figure S14. The UV-vis-NIR transmittance spectra (a), T_{sol}, and T_{NIR} diagram (b) of the BSW without Au film in the process of incident angle θ increase.
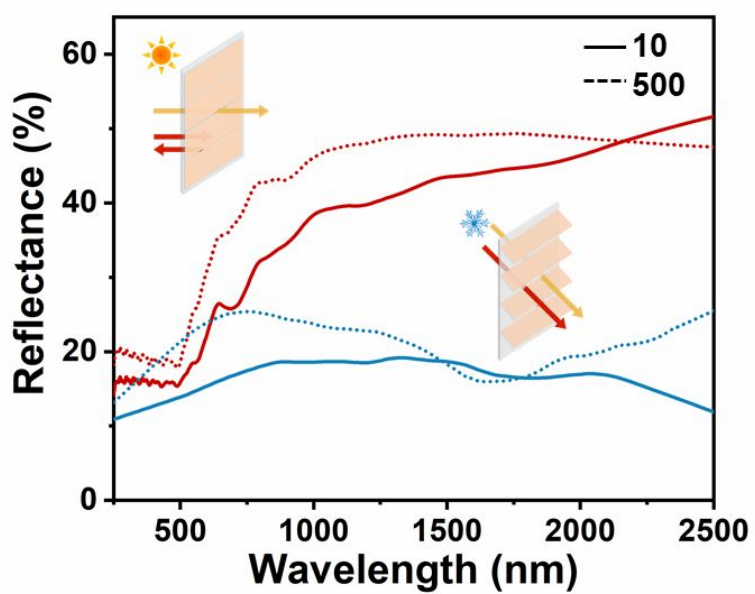
Figure S15. Simulated UV-vis-NIR reflectance spectra of the BSW with a period of 10 μm and a period of 500 μm in summer and winter.

$$S_{p1} = S_{a1} \qquad S_{p1} = 3S_{a2}$$

Figure S16. The schematic illustration of projection area for the BSW with both tens and hundreds of microns period in normal light direction.

$S_{p1} = S_{a1} (\cos\beta - \sin\beta \cdot \tan\theta)$ $S_{p2} = 3S_{a2} (\cos\beta - \sin\beta \cdot \tan\theta)$
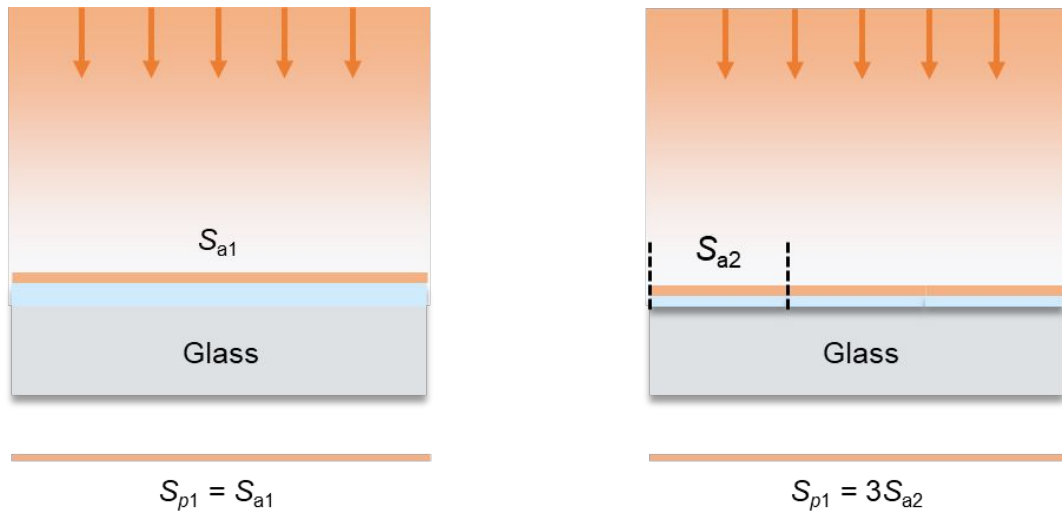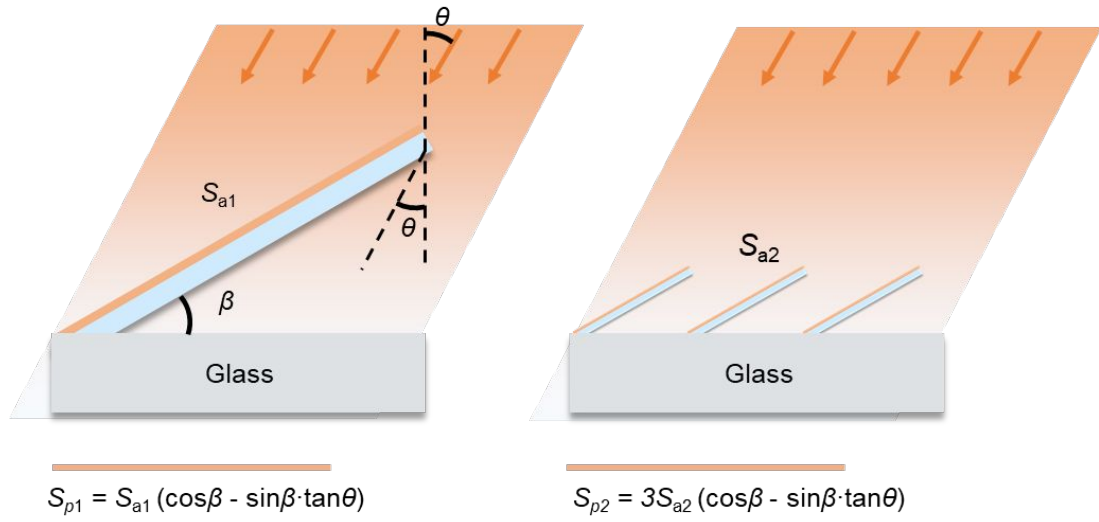
Figure S17. The schematic illustration of projected area for for the BSW with both tens and hundreds of microns period in oblique light direction.
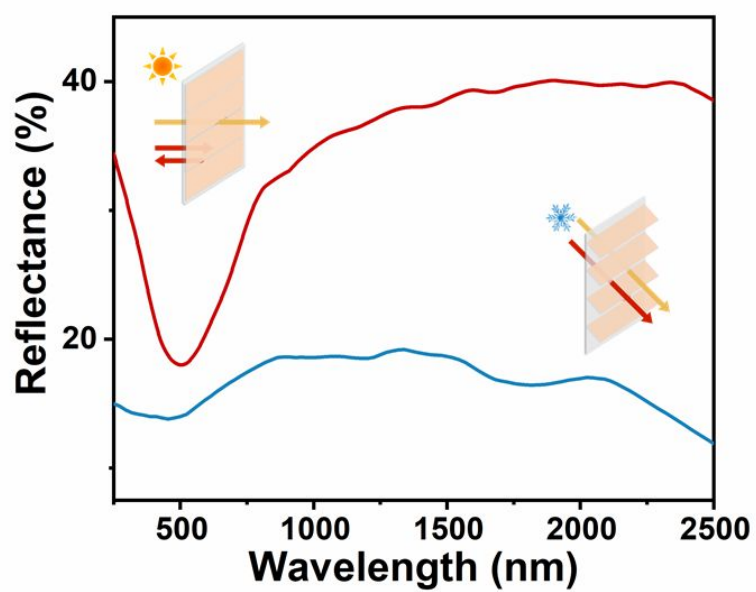
Figure S18. UV-vis-NIR reflectance spectra of the BSW in summer and winter.
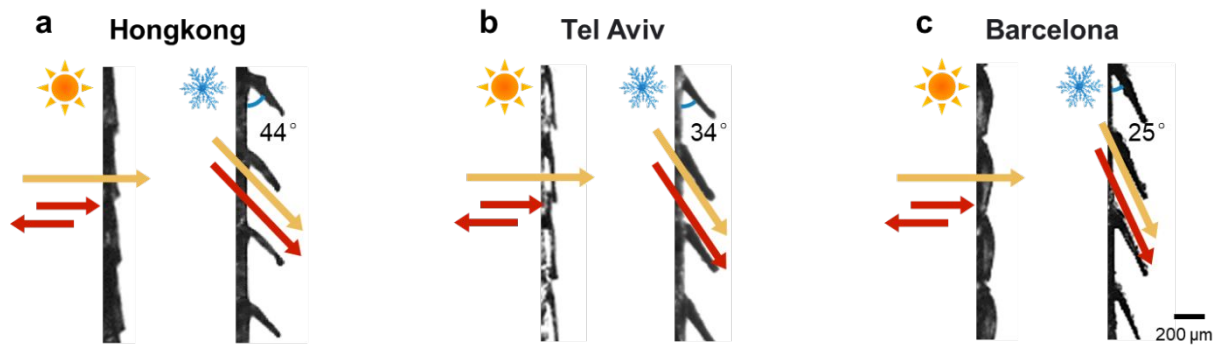
Figure S19. The optical images of the BSW custom designed for Hongkong (a), Tel Aviv (b) and Barcelona (c), respectively. For the three locations, there are three BSWs with different original tilted configurations. If the BSW is custom designed for Hongkong, the angle of the original tilted configuration is 44º. After being treated into the temporary shape of flat topography, the BSW can recover to the original tilted configuration with 44º tilted angle upon heating.

Figure S20. The annual energy consumption of the three windows in Hongkong, Tel Aviv and Barcelona, respectively.

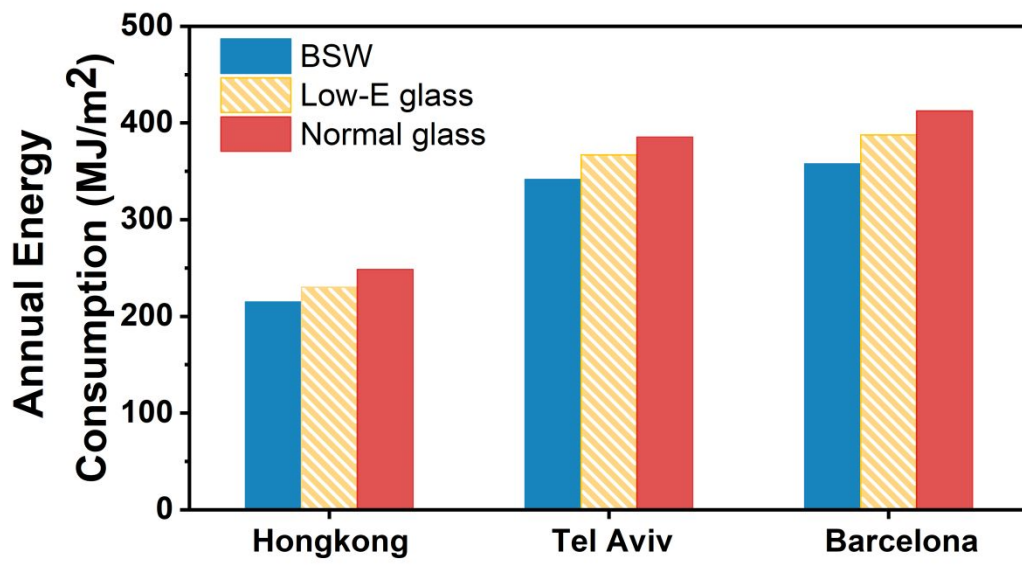**Table S1:** Parameters of the normal glass, commercial low-E glass and the BSW used for the energy consumption simulation.

Name	Normal glass	Commercial Low-E glass	BSW			
			Summer	Winter		
				Hongkong	Tel Aviv	Barcelona
Thickness (m)	0.003	0.003	0.003	0.003	0.003	0.003
Solar Transmittance at Normal Incidence	0.837	0.510	0.434	0.763	0.774	0.761
Front Side Solar Reflectance at Normal Incidence	0.075	0.0742	0.279	0.0553	0.0525	0.0608
Back Side Solar Reflectance at Normal Incidence	0.075	0.0832	0.365	0.0897	0.0923	0.107
Visible Transmittance at Normal Incidence	0.898	0.655	0.651	0.794	0.782	0.788
Front Side Visible Reflectance at Normal Incidence	0.081	0.0613	0.146	0.0523	0.0517	0.0539
Back Side Visible Reflectance at Normal Incidence	0.081	0.0763	0.232	0.0815	0.0856	0.086
Infrared Transmittance at Normal Incidence	0	0	0	0	0	0
Front Side Infrared Hemispherical Emissivity	0.84	0.98	0.84	0.84	0.84	0.84
Back Side Infrared Hemispherical Emissivity	0.84	0.4	0.35	0.62	0.54	0.41
Conductivity (W/m*K)	0.9	0.9	0.17	0.17	0.17	0.17

Reference:

(1) Chen, H.; Baitenov, A.; Li, Y.; Vasileva, E.; Popov, S.; Sychugov, I.; Yan, M.; Berglund, L., Thickness Dependence of Optical Transmittance of Transparent Wood: Chemical Modification Effects. *ACS Appl. Mater. Interfaces* **2019**, *11*, 35451−35457.